

https://dspace.org/

The effect of blasting on the rockmass for designing the most effective preconditioning blasts in deep-level gold mines

Toper, Ali Zafer

2011-04-18
http://hdl.handle.net/10539/9499

Downloaded from a DSpace repository. https://dspace.org/

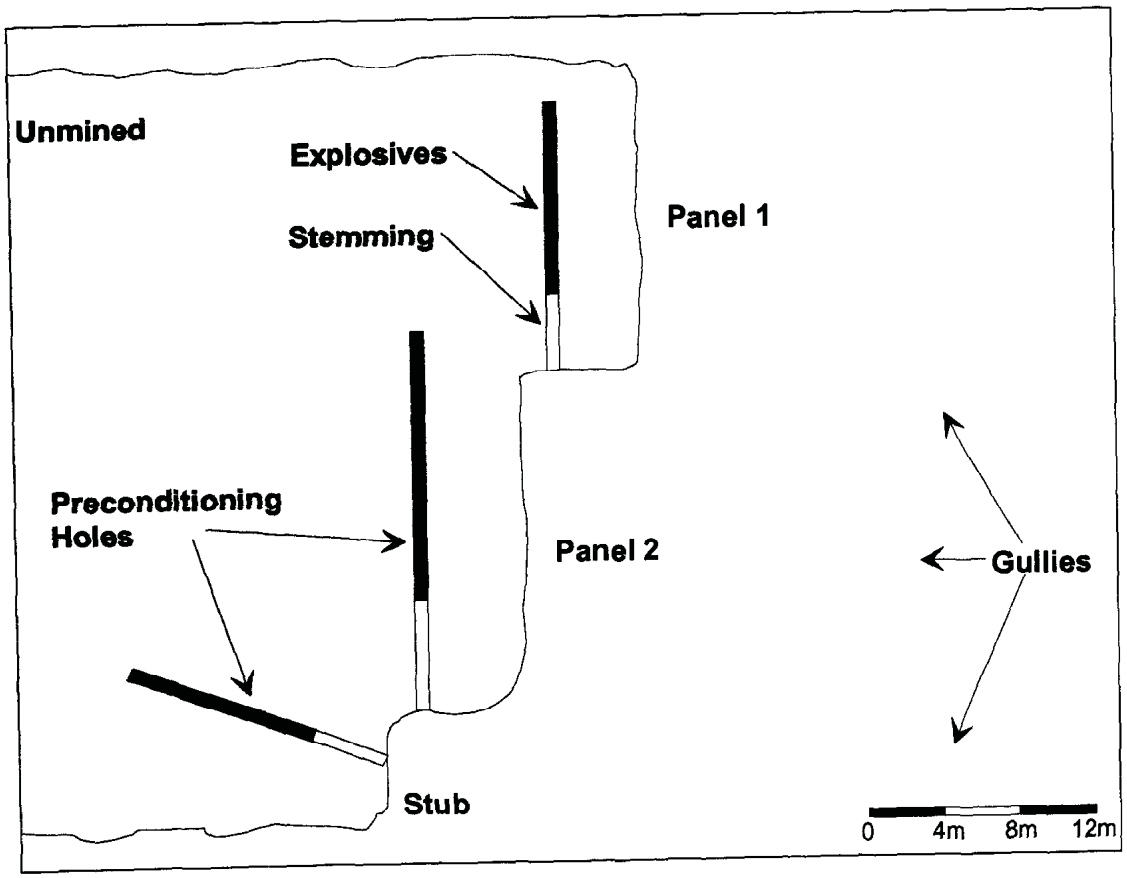


Figure 4.2.2 Preconditioning layout at the test site (17-24W stope)

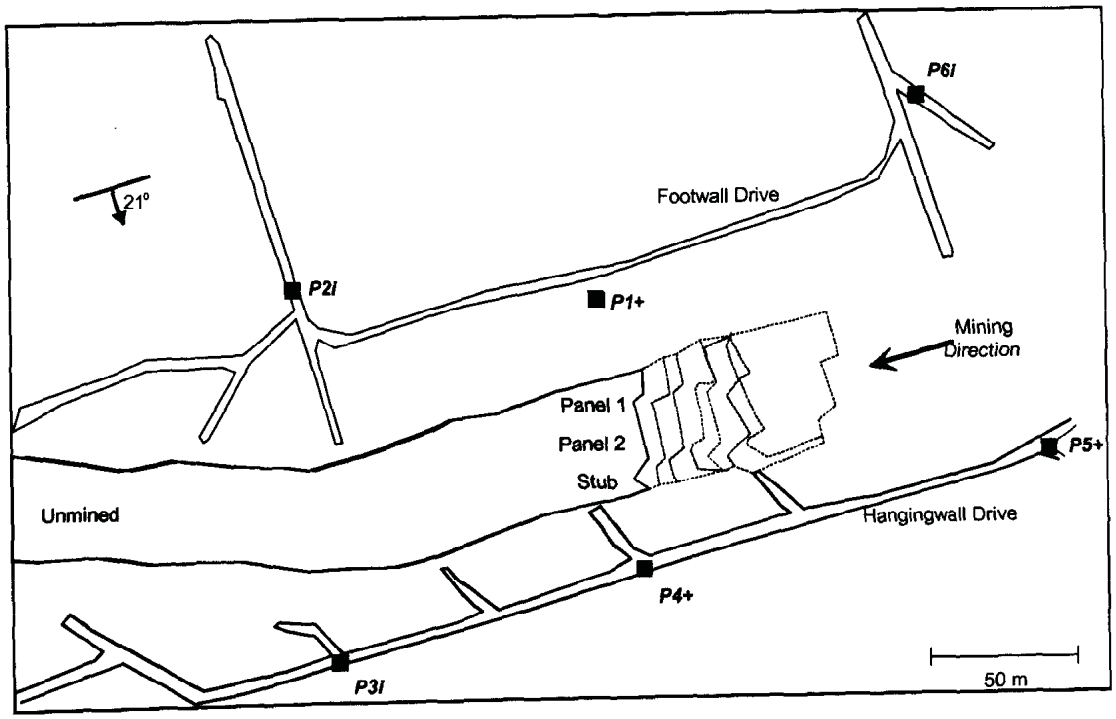


Figure 4.2.3 Plan of the preconditioning test site, showing the geophone positions for the PSS network

The PSS network had a fairly good location accuracy (5.4 ± 3.0 metres) for seismic events that originated from the preconditioning site. This location accuracy provided a high degree of confidence to studies of migratory patterns of microseismic event locations ahead of the mining faces. These migratory patterns were related to the stress redistribution that took place in the rockmass during mining and preconditioning activity. This formed an important part of the analysis of the effectiveness of preconditioning.

Convergence measurements

Convergence data was acquired with the use of convergence stations by measuring the distances between bolts installed in the hangingwall and footwall. Through triangulation, daily measurements were resolved into the principal convergence and ride components of ground movement (Piper and Gürtunca, 1987).

The maintenance of convergence stations at the test site was a problem because of deteriorating ground conditions in the back areas and the rapid convergence rate close to the faces. Stations often became inaccessible 8 m from the face. Despite these difficulties, a large database of convergence measurements within 10 m of the faces was collated, and the rockmass response in the form of ground movement was analysed.

Ground motion monitoring

The Ground Motion Monitor (GMM), known as the "Black Box", was used to record the ground accelerations during face-parallel preconditioning. These recorded ground accelerations for each preconditioning blast were compared to the seismic data obtained from the PSS, the convergence measurements and the observations of the change in ground conditions after the blast. The "Black Box" was intended to remove the subjectivity from the observations of the face condition and to provide measured values of the ground response to the preconditioning blast. This allowed, at least partially, the evaluation of the effects of the stemming of the preconditioning hole and beyond the end of the hole in situations where the hole was drilled shorter than the face length.

4.2.4 Summary of preconditioning activity

During the preconditioning experiment, 3724 square metres of ground was mined with 51 preconditioning blasts over a period of 39 months. This corresponds to a total of 93 metres of face advance, which is an average of 2.39 metres per month. A total of 4328 kg of explosive was used. The total length of preconditioning holes drilled was 722 m and an average of 85 kg of explosive was used in each preconditioning hole. The average time between preconditioning blasts was 24 days, and this was maintained fairly consistently throughout the test period.

4.2.5 Analysis of preconditioning blasts

A number of criteria were used in the assessment of the effectiveness of each preconditioning blast at the 17-24W preconditioning site. These criteria were developed in an attempt to minimise subjectivity in the assessments. The criteria were:

- the seismic magnitude of the recorded blast event;
- the number of seismic events recorded from the site in the 24 hours following the blast;
- the magnitude of the largest event in the subsequent seismicity;
- the degree of spatial migration evident in the subsequent seismicity; and
- the convergence recorded on the following day.

In the assessment, account was taken of:

- the amount of explosive used in the blast;
- whether or not there was a production blast in another panel on the same day; and
- whether the convergence measurement was made in the panel of the preconditioning blast or in another panel.

The rating system which was developed is outlined in Appendix A. Appendix B contains a detailed summary of all preconditioning blasts which were detonated

at the preconditioning site during the experiment, and includes a rating for each blast. Note that the rating system was conservative, so that an acceptable preconditioning blast was one that scored 30 per cent or more. A very effective blast scored 50 per cent or more. The average rating for all preconditioning blasts was 38 per cent, with 70 per cent of preconditioning blasts having scored 30 per cent or more. The average ratings by panel are given in Table 4.2.1.

Table 4.2.1 Summary of preconditioning blast ratings per panel

	Average rating (%)	Blasts above 30% rating (%)
Stub	28	40
Panel 1	40	79
Panel 2	41	76
Total for the pillar	38	70

It is clear from Table 4.2.1 that preconditioning blasts set off in panels 1 and 2 were typically more effective than those set off in the stub. This was related to the orientation of the preconditioning holes in the stub and to the fact that shorter preconditioning holes with less explosive were used in the blasts there. The relative lack of effectiveness of the stub blasts was a source of concern, as this area of the pillar was the site of a substantial concentration of stress, which might be aggravated by the effective preconditioning of panels 1 and 2.

The preconditioning blasts with low ratings (20 per cent or less) generally followed inadequacies in the preparation of the blast (incorrect hole positioning or orientation, drilling difficulties, insufficient stemming, etc.). Other ineffective blasts were produced by short or small-diameter holes with less explosive, especially for the blasts in the stub.

The average rating for the 33 preconditioning blasts which were set off without any concurrent production activity was 41 per cent. The average rating for the 18 preconditioning blasts, which were followed by at least one production blast in another panel on the same day was 34 per cent. This result indicated that if a production blast took place in a neighbouring panel on the same day as a

preconditioning blast it had little effect on the results of the preconditioning process.

4.2.6 Quantitative analysis of the effects of preconditioning

In order to quantify the effects of face-parallel preconditioning on the rockmass response, on the level of seismicity, rockburst incidences, general ground conditions and safety while mining the stability pillar at the experimentation site, the following objective methods were used:

- an analysis of seismic activity;
- an analysis of triggering effect of preconditioning;
- convergence monitoring;
- ground motion monitoring;
- an assessment of face dilation;
- an analysis of mining-induced fracturing; and
- seismic tomography.

Analysis of seismic activity

The full seismic history of all but three of 51 face-parallel preconditioning blasts was recorded by the monitoring PSS. This history included the blasts themselves, as well as the seismicity occurring at the site in the 24 hours following each blast. The monitoring and analysis of seismicity allowed the development of a considerable understanding of the processes occurring in the rockmass in response to preconditioning blasts.

About 80 percent of the recorded preconditioning blasts were detected as events with seismic magnitudes in the range of:

M = (Mass of explosive (kg) / 100) ± 0.5.....(2)

where "mass of explosive" used for the blast is given in kilograms (Figure 4.2.4). This gives a seismic efficiency of about one percent. Two of the recorded

preconditioning blasts had magnitudes above this range, indicating a release of stored strain energy from the rockmass in addition to that would arise from the normal interaction of the explosive with the rock. The rockmass in the vicinity of these two blasts had clearly been carrying excess load, which was relieved by the preconditioning. Eight of the recorded preconditioning blasts had magnitudes below the range given above. These were mostly blasts from short holes with small quantities of explosive, or blasts from incorrectly laid-out holes or holes that had proved difficult to drill and that had not been drilled to the planned length.

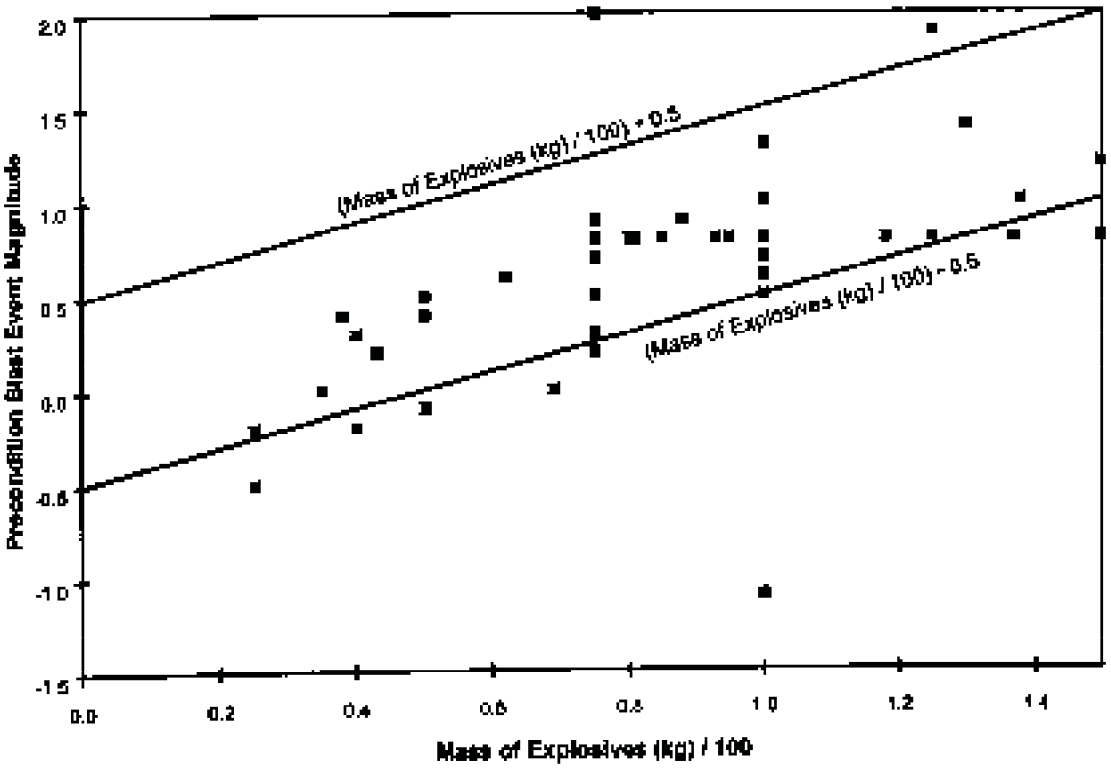


Figure 4.2.4 Comparison of the recorded preconditioning blast event magnitudes with the amount of explosive used for each blast

The seismic data showed that effective preconditioning blasts induce stress transfer away from the preconditioned area, release stored strain energy from the rockmass and can beneficially affect the stress concentrations in areas of the rockmass adjacent to the preconditioned area. The seismic expression of preconditioning in a rockmass includes the blast event itself, an increase in the rate of induced microseismicity following the blast, and the triggering of any separate larger seismic events by the blast. A few specific case examples are given below:

Case 1: The recorded microseismicity following effective preconditioning blasts exhibits spatial migration away from the vicinity of the preconditioning blasts, indicating the transfer of stress further ahead of the face of the preconditioned panel and towards unpreconditioned ground. Figure 4.2.5 shows an example of the effects of a preconditioning blast that took place on 26 November 1992. The star in Figure 4.2.5 (a) shows the location of the blast event (M = 0.7) as recorded by the PSS. The arrow in Figure 4.2.5 (b) indicates the spatial migration of microseismicity (circles) recorded by the PSS in the 24 hours following the blast. This seismicity showed a clear migratory trend away from the top panel towards the panels below, indicating the transfer of stress away from the panel after the preconditioning blast.

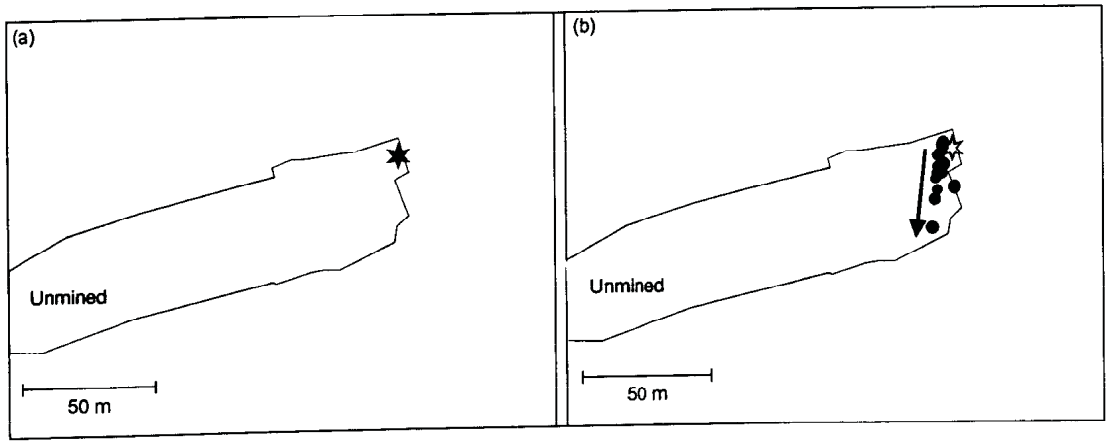


Figure 4.2.5 Seismic data recorded during and following a preconditioning blast at the test site on 26 November 1992

Case 2: Figure 4.2.6 shows an example similar to that shown in Case 1. The star in Figure 4.2.6 (a) shows the location of the blast event (M = 1.0) as recorded by the PSS. In Figure 4.2.6 (b) the arrows indicate the spatial migration of microseismicity recorded by the PSS in the 24 hours following the blast. This seismicity concentrated further ahead of the preconditioned panel (i.e. away from the working areas), as well as in the adjacent panel above, indicating the transfer of stress away from the vicinity of the preconditioning blast. This example illustrates the need for a correct sequencing of the preconditioning of adjacent panels. Since the preconditioning blast in this panel transferred some of the stress onto the panel above, it was thus important that the panel above had been

preconditioned (destressed) prior to this panel, or the stress transfer might have loaded the rockmass ahead of panel above and led it to failure.

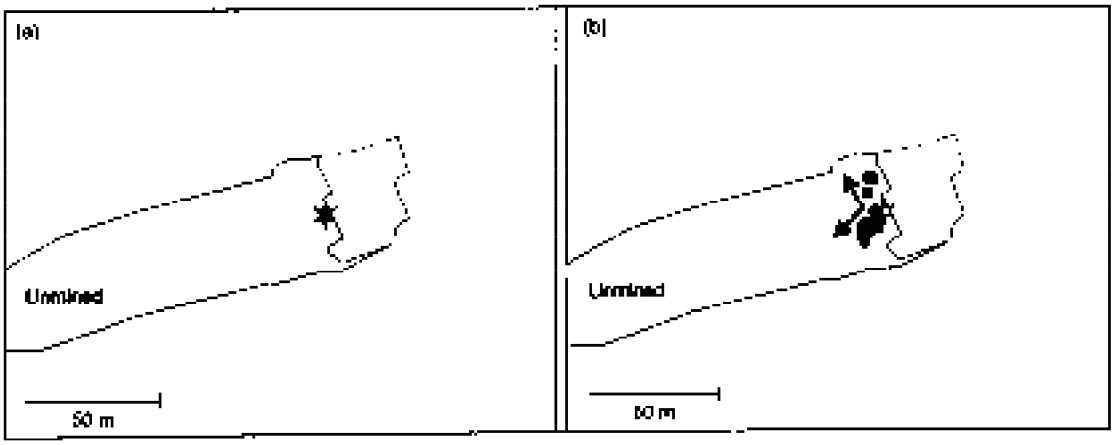


Figure 4.2.6 Seismic data recorded during and following a preconditioning blast at the test site on 22 December 1993

Case 3: Effective preconditioning blasts have been found to release stored strain energy from the rockmass through the triggering of separate larger seismic events. While these have resulted in some damage to the working areas on occasion, it is significant that the events were triggered at a time when there were no workers in the stope, so that the strain energy which had built up in the rockmass ahead of the stope faces in response to the mining activity was released without injury to workers. The star in Figure 4.2.7 (a) shows the location of the preconditioning blast event (M = 0.8) as recorded by the PSS on 31 March 1993. This preconditioning blast facilitated the release of stored strain energy by triggering an additional event (M = 0.4) in the same panel. The white star in Figure 4.2.7 (b) indicates the location of this event. The subsequent microseismicity (circles in Figure 4.2.7 (b)) migrated away from the preconditioned panel, indicating that the vicinity of the blast had been effectively destressed.

Case 4: Through the mechanism of stress transfer in the rockmass, effective preconditioning blasts alter the stress concentrations in adjacent areas.

There was a three-month production stoppage from July to September 1994, and it was decided to precondition all three faces before restarting the production

activity at the site. The first of those blasts, on 20 September 1994 in the top panel, went according to plan and was effective in preconditioning the rockmass ahead of the panel face. But, due to some drilling difficulties, neither of the preconditioning blasts, in the middle panel on 26 September and in the stub on 29 September, produced a discernible preconditioning effect. Thus, the top panel preconditioning blast on 28 October 1994 took place at a time when neither the middle panel nor the stub had been effectively destressed.

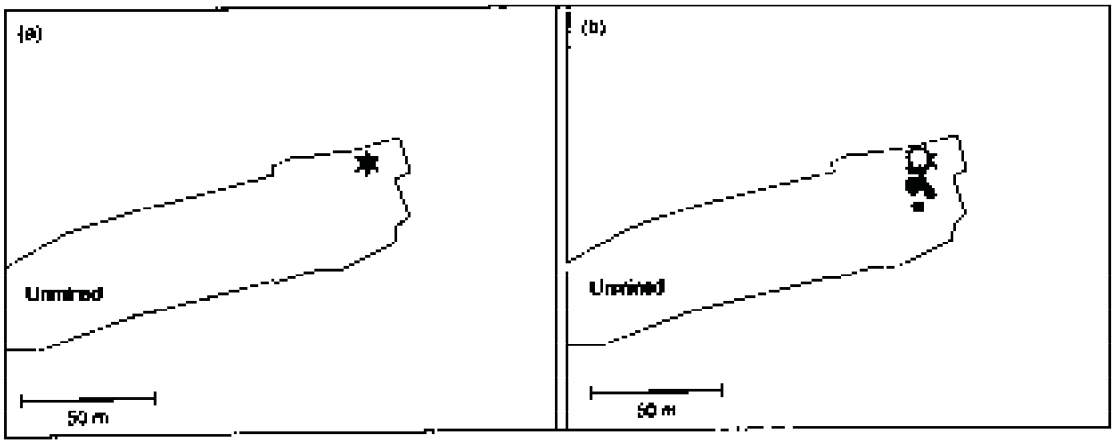


Figure 4.2.7 Seismic data recorded during and following a preconditioning blast at the test site on 31 March 1993

The preconditioning blast on 28 October 1994 was recorded as an M = 0.9 seismic event by the PSS. The star in Figure 4.2.8 (a) shows the location of this event. The subsequent microseismicity (circles in Figure 4.2.8 (b)) migrated down-dip, indicating the transfer of stress away from the preconditioned panel. The addition of load to the rockmass ahead of the panel below then triggered a large (M = 2.1) seismic event in that area, releasing the strain energy that had accumulated there. The white star in Figure 4.2.8 (c) indicates the location of this triggered event. The destressing of both panels in sequence suggests that additional load was then being carried by the rockmass ahead of the stub face, a supposition borne out by the subsequent triggering of a large (M = 1.5) seismic event in that area by the production blast in the stub face. The white star in Figure 4.2.8 (d) shows the location of this triggered event. All of the mining faces were thus effectively destressed by the one preconditioning blast in the top panel, on that occasion.

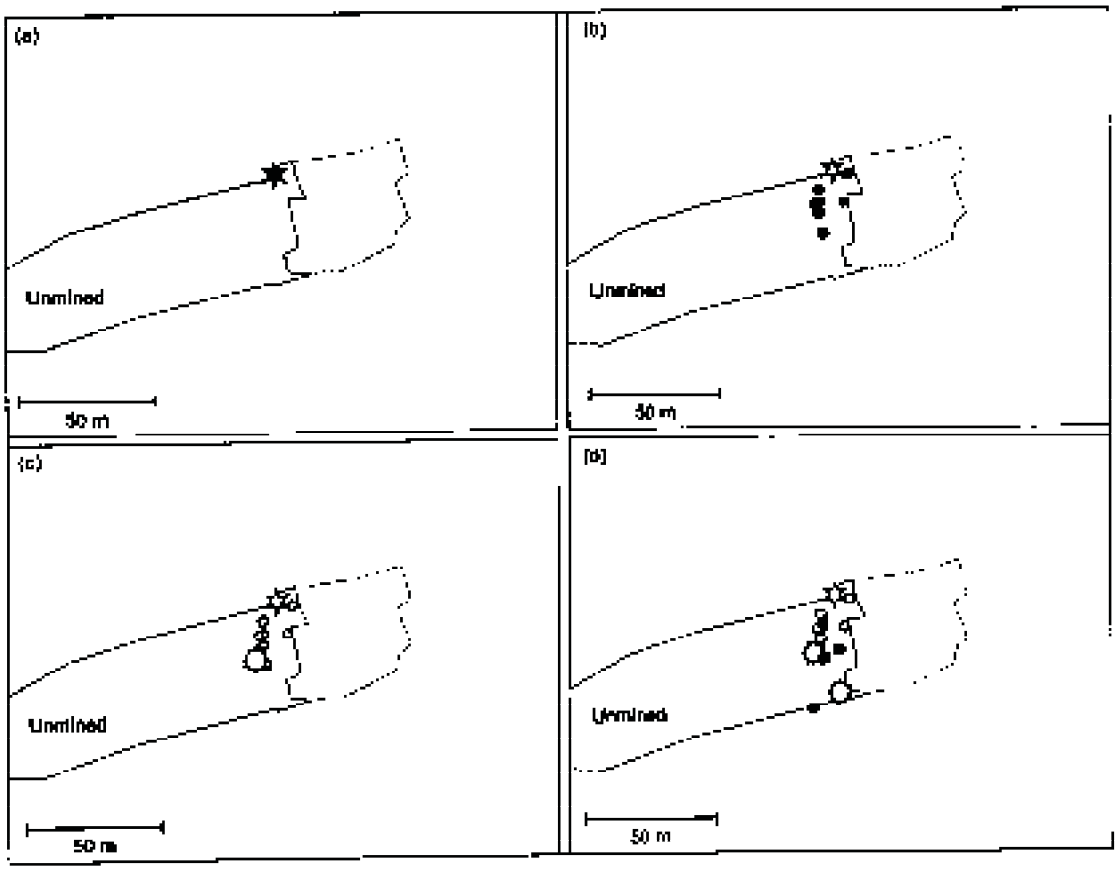


Figure 4.2.8 Seismic data recorded during and following a preconditioning blast at the test site on 28 October 1994

Case 5: The preconditioning blast in the top panel took place on 10 January 1995. The star in Figure 4.2.9 (a) shows the location of the blast event (M = 0.7) as recorded by the PSS. The circles in Figure 4.2.9 (b) show the microseismicity recorded following the blast and indicate the stress transfer away from that panel towards the panel below. A production blast in the middle panel face on the following day then triggered the instability that had developed in the rockmass ahead of the panel, releasing the stored strain energy by way of two large (M = 1.7) seismic events. The darker circles in Figure 4.2.9 (c) show the microseismicity recorded following the production blast and two white stars in Figure 4.2.9 (c) show the location of the triggered seismic events.

While well-executed preconditioning blasts have been proved to have very beneficial effects on the stress state and condition of the rockmass ahead of a stope face, it is important to note that poorly executed preconditioning blasts were either ineffective or negatively affected the stress state of a rockmass.

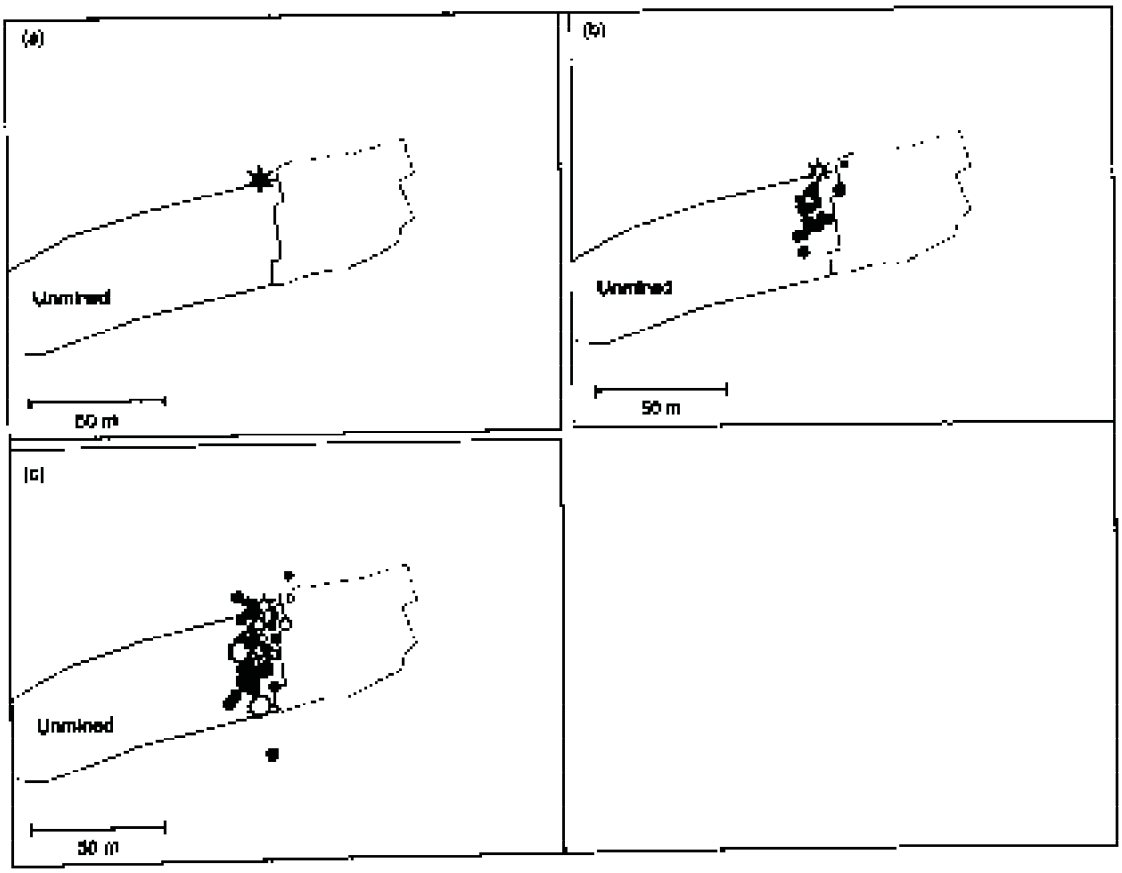


Figure 4.2.9 Seismic data recorded during and following a preconditioning blast at the test site on 10 January 1995

Defective preconditioning blasts due to the drilling of the face-parallel preconditioning holes too far ahead of the face either had no effect on the stress condition at the face or, in the worst case, actively added to the load carried by the face. Seismically, the results of the preconditioning blasts set off too far ahead of the face were small blast events, little induced microseismicity, and no triggering of larger seismic events.

On occasion, drilling difficulties have necessitated the abandonment of a preconditioning hole before it was completed, requiring the drilling of a second hole in close proximity to the first. In a number of such cases, even though the first hole was grouted closed, the results of the preconditioning blast have been unsatisfactory. There has been clear physical interaction between the holes during the blast, often with a significant amount of blow-out damage between the collars of the holes. While the blasts themselves have generally been adequate as shown by the magnitude of the recorded blast event, there has been little

induced microseismicity and no triggering of larger seismic events by the blast, indicating a lack of interaction of the blast with the stress field in the rockmass ahead of the stope face.

Case 6: An example that serves to illustrate the importance of correct sequencing is the pair of preconditioning blasts that were set off in April 1994. The preconditioning blast of 11 April 1994 was set off in the stub without the panel above having been preconditioned beforehand. The star in Figure 4.2.10 (a) shows the location of the blast event (M = 0.4) as recorded by the PSS.

The stub preconditioning hole was oriented effectively perpendicular to the stope face, with the intention of remobilising the pillar-edge parallel fractures that were prominent ahead of the stub face. The result was that the preconditioning blast was effective further ahead of the face than it would have been had the hole been oriented parallel to the face. The net effect was to drive the stresses back towards the face, mostly in the area between the stub and the middle panel. The circles in Figure 4.2.10 (b) show the microseismicity recorded following the blast. This area is generally not effectively preconditioned, due to the geometric effect of the stemming near the collars of the stub and middle-panel preconditioning holes.

The three production blasts which took place over the following days do not appear to have altered the stress state between the middle panel and the stub significantly. The circles in Figure 4.2.10 (c) show the microseismic events associated with these production blasts.

On 15 April 1994, a preconditioning blast was set off in the panel above the stub. The star in Figure 4.2.10 (c) shows the location of the blast event (M = 1.4) as recorded by the PSS. This seems to have had the effect of adding further to the stress which had concentrated in the area and a large (M = 2.3) damaging seismic event resulted, located on the face between the middle panel and the stub. The white star in Figure 4.2.10 (d) shows the location of this triggered seismic event.

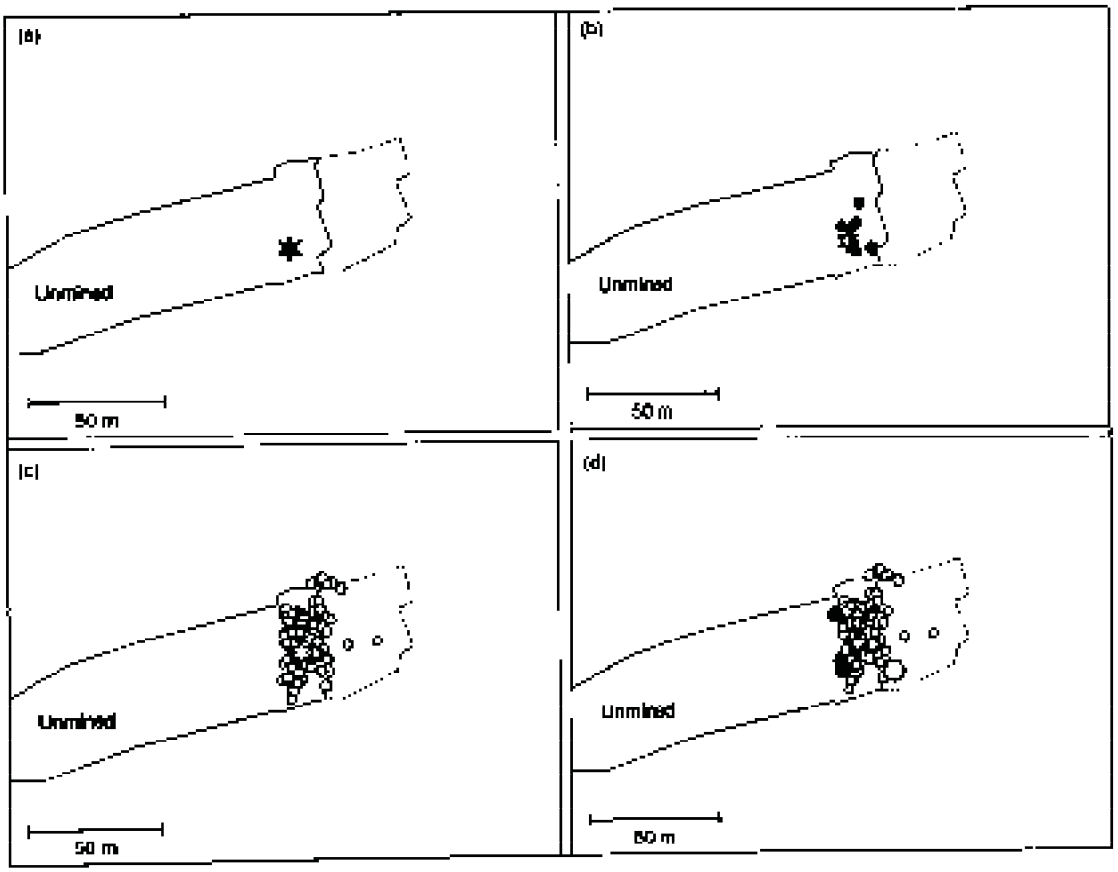


Figure 4.2.10 Seismic data recorded during and following the preconditioning blasts at the test site on 11 April and 15 April 1994

Analysis of triggering effect of preconditioning

During the three-and-a-half years of face-parallel preconditioning, 48 large (M ≥1.0) seismic events were recorded in the vicinity of the 17-24W preconditioning site. Table 4.2.2 summarises the various triggering conditions associated with the large events. Of these, 45 were located less than 50 m ahead of the stope face and the other three events were located within the core of the pillar, between 50 and 100 m ahead of the faces. Twenty-four of these 45 events occurred during blasting time and the majority of the remainder occurred within a few hours thereafter. In fact, some 40 of the 45 events were associated with a clearly recognisable trigger mechanism, in the form of the preconditioning blast or production blast. The remainder probably resulted from the accumulation of stress via time-dependent effects at work in the rockmass ahead of the advancing faces. Four larger events took place during the day shift, when

workers were present in the stope, but none of these resulted in injury to any of the workers.

Table 4.2.2 shows that 44.4 percent of the 45 larger seismic events were associated with preconditioning activity in some way. This included the blasts themselves being recorded as large events, as well as the direct or indirect triggering of separate large events by preconditioning. On the other hand, 46.7 percent of the larger events were triggered by production blasting. Given that there were a total of 51 preconditioning blasts set off at the site, compared with six times that number (317) of full-face production blasts, the preconditioning was clearly more efficient in terms of the triggering of larger seismic events, and thereby the controlled release of stored strain energy from the rockmass, than was the normal production activity. Table 4.2.3 compares the preconditioning and the production triggering rates in more detail.

Table 4.2.2 Occurrence of large (M ≥1.0) seismic events of the preconditioning site

	Number of events	Percentage of total
Recorded preconditioning blasts	7	15.6
Triggered (preconditioning only)	5	11.1
Triggered (preconditioning & production)	2	4.4
Triggered (production after preconditioning) [1]	5	11.1
Not directly triggered (after preconditioning) [1]	1	2.2
Subtotal: Related to preconditioning	20	**44.4**
Triggering (production only)	21	46.7
Not triggered	4	8.9
Total within 50 m of stope face[2]	45	**100.0**

[1] within 2 days of preconditioning blast

[2] excludes 3 events in core of pillar

While the numbers in Table 4.2.2 are given in terms of the total number of large events, those in Table 4.2.3 are given in terms of the total number of

preconditioning and production blasts associated with those large events. On several occasions, single preconditioning or production blasts have triggered multiple large events. From Table 4.2.3, it is clear that preconditioning blasting was more efficient than production blasting in terms of the triggering of large seismic events.

Table 4.2.3 Occurrence of large (M ≥1.0) seismic events in association with preconditioning and production activity

		Triggering *blasts*	Total blasts	Triggering *percentage*
Preconditioning	Panel 1	[1] 2	19	10.5
	Panel 2	[1] 6	22	27.3
	Stub	[1] 2	10	20.0
	Total	**10**	**51**	**19.6**
Production	Panel 1	1	[2] 104	1.0
	Panel 2	13	[2] 108	12.0
	Stub	8	[2] 105	7.6
	Total	21	317	6.6

[1] *includes M. ≥1.0 blast events*

[2] *full-face blasts only*

Clearly, well-controlled preconditioning blasts redistributed stresses effectively and also served to control the timing of the release of stored strain energy from the rockmass. Poorly controlled preconditioning blasts, on the other hand, either did not redistribute stress effectively or acted to induce unfavourable stress redistribution (i.e. moving the stress towards the face of the "preconditioned" *area, rather than away from it*). Actual preconditioning blasts that were set off too far ahead of the face, in the region of highly confined rock, did not induce any observable stress changes in the rockmass. However, some larger seismic *events that were located further* ahead of the face than the usual position of a preconditioning hole induced unfavourable stress redistribution by effectively destressing the source region and driving the stress back onto the closest panel face. *While preconditioning clearly cannot control* the larger-scale behaviour of

the pillar (larger seismic events will continue to occur as the rockmass of the pillar responds to the stress changes induced by mining), preconditioning was very effective in the vicinity of the stope faces, both in terms of the relaxation of stress there and in terms of the creation of a "buffer" zone, which served to reduce the adverse effects of larger seismic events on the working areas.

Convergence measurements

The daily convergence rates for production and preconditioning blasts are compared in Table 4.2.4. All measurements were taken within less than 10 metres of the advancing face. The average convergence for the production blasts is based on nearly 100 data entries, but the preconditioning database is more limited with fewer than 10 entries for each result quoted.

Table 4.2.4 Average induced daily convergence as a result of production and preconditioning blasting

		Convergence Rate (mm/day) measured at		
		Panel 1	Panel 2	Stub
Production blast at	Panel 1	9.6 ± 4.2	6.0± 3.6	3.0 ± 2.3
	Panel 2	5.3 ± 7.1	23.1 ± 19.5	14.4 ± 9.6
	Stub	4.2 ± 6.1	6.8 ± 9.0	9.3 ± 3.8
No blast		2.4 ± 1.3	3.8 ± 2.4	2.8 ± 1.6
Preconditioning blast at	Panel 1	18.3 ± 13.7	5.0 ± 3.9	***
	Panel 2	12.1 ± 11.2	28.0 ± 19.1	***
	Stub	14.2 ± 13.8	***	***

*** Insufficient Data

A production blast in a panel had a great effect on the convergence rate of that panel and a reasonably limited effect on the adjacent panels. Preconditioning blasts from holes positioned 5 m ahead of the face had a greater effect on the convergence than did the production blasts. This was especially evident from the convergence recorded after a preconditioning blast in the panels other than the one actually being preconditioned. This is due to the more global effect of the

preconditioning blast which was indirectly achieved as a result of stress transfer onto unpreconditioned ground. The high standard deviations reported for the preconditioning blasts were due largely to the variability in the conditions in which the blasts were carried out. Several blasts had been less successful than expected, resulting in a lower convergence and others had triggered large events, resulting in a very large convergence in all panels.

Ground motion monitoring

Despite the fact that only six preconditioning blasts had taken place with the ground motion monitors installed, specific responses were apparent. Ground accelerations recorded within the charge length of the hole were in excess of 1000 m/s^2 with the waveforms being saturated. The effects of the blasts appeared to diminish quite dramatically beyond the charge in the hole. The ground accelerations measured at the top end of the hole (~336 m/s^2) and at the collar side (~238 m/s^2) were considerably less than those measured towards the centre of the charge.

Dilation of stope face

An effective preconditioning blast resulted in scaling of rock off the face and shake-out of loose rock from the hangingwall. The extent of this depends largely on the fractured nature of the rock and the extent of barring undertaken by the stope crew. On several occasions, however, a considerable amount of dilation was noted on the face (Figure 4.2.11), providing more evidence to support the model of preconditioning (Lightfoot, 1993; Lightfoot, *et al.*, 1994; and Kullmann, *et al.*, 1994) and its interaction with the rockmass. Dilation of the face is clearly indicated by the open fractures enhanced by paint lines initially applied for a Ground Penetrating Radar (GPR) scan before the blast. Scaling of rock from the face resulted in the removal of paint lines on both sides of this area as shown in Figure 4.2.11. The amount of dilation, however, is extremely difficult to quantify, with any degree of accuracy, using conventional measuring techniques.

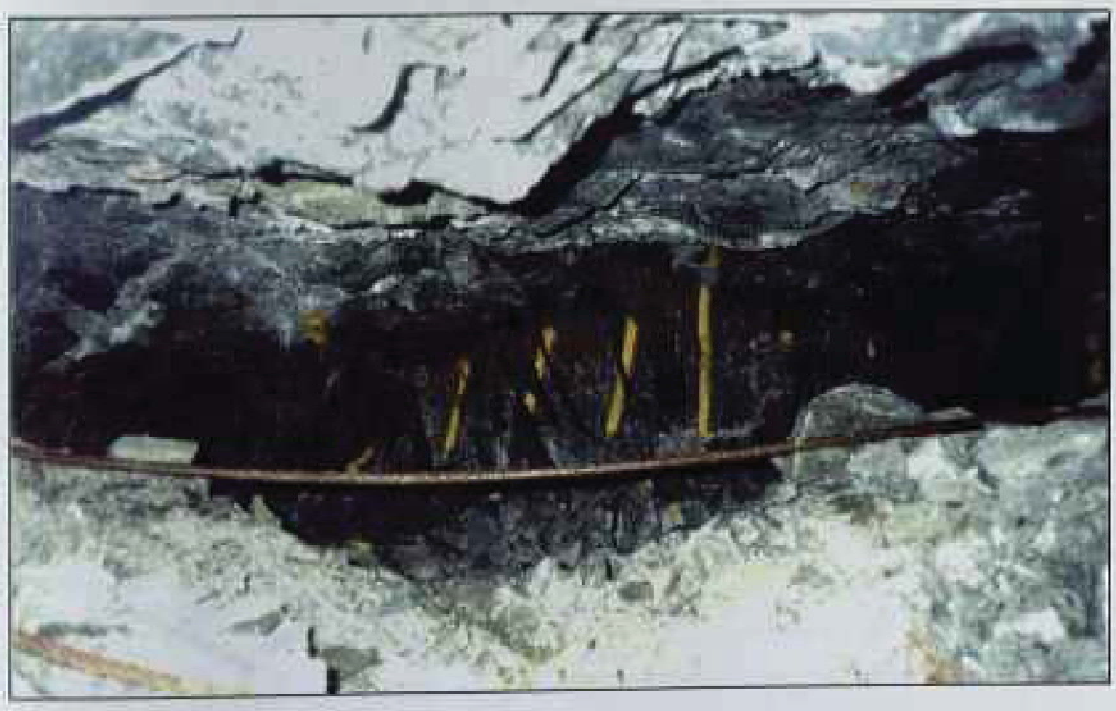


Figure 4.2.11 The stope face appearance after a preconditioning blast

In order to quantify the amount of dilation of the face into the open stope and the opening up of pre-existing fractures, a technique called digital photogrammetry was used underground. Images of the face were captured, with the use of a high-resolution digital camera, before and after the preconditioning blast (Figure 4.2.12). However, the biggest constraint in the use of this technique for underground analysis was in providing a fixed control point to establish a co-ordinate reference system. Since no point near the face remains fixed relative to any other point, especially after a blast, the results could only be evaluated on the basis of certain assumptions (Figure 4.2.13).



to the face. Underground these are observed as low-persistence joints occasionally with calcite infill of up to 2 mm thickness.

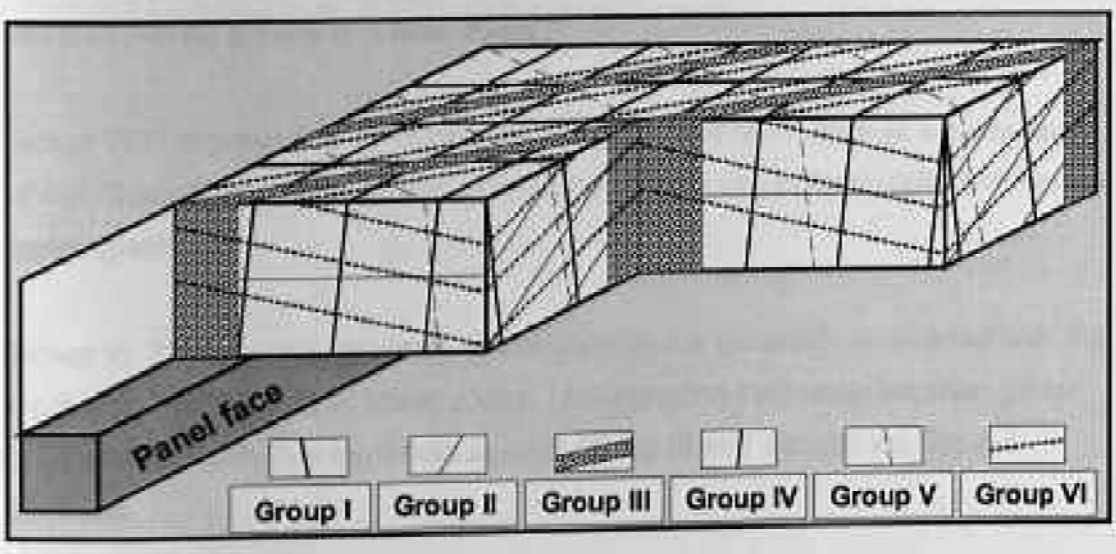


Figure 4.2.14 Schematic view of fracture groups (not to scale)

Group II: As the second major cluster, this group also lies more or less perpendicular to the face, but has a shallower dip of between 50° and 60°. These are sinuous joints, often vein-quartz filled and are faults that appear to interconnect the fractures of Group III.

Group III: This group of fractures lies at an angle of 35° to 45° to the panel face. The fractures in this group are clustered into distinctive steeply dipping highly sheared zones containing both calcite and vein quartz. These shear zones are between 50 cm and 80 cm wide and occur at intervals of about 3 m. White crushed quartzitic gouge is also common in these fractures, which show several phases of movement. Fractures in this group have an orientation that is consistent with the regional trend of the dykes and faults across the mine. This suggests that the initial alignment of these fractures was strongly influenced by regional-scale tectonics. At a very late stage, probably due to current stoping and preconditioning, these fractures were abraded to form a fine white quartzitic gouge.

Group IV: This group consists of steeply dipping joints that are orientated approximately parallel to the panel face. These joints have a fairly low

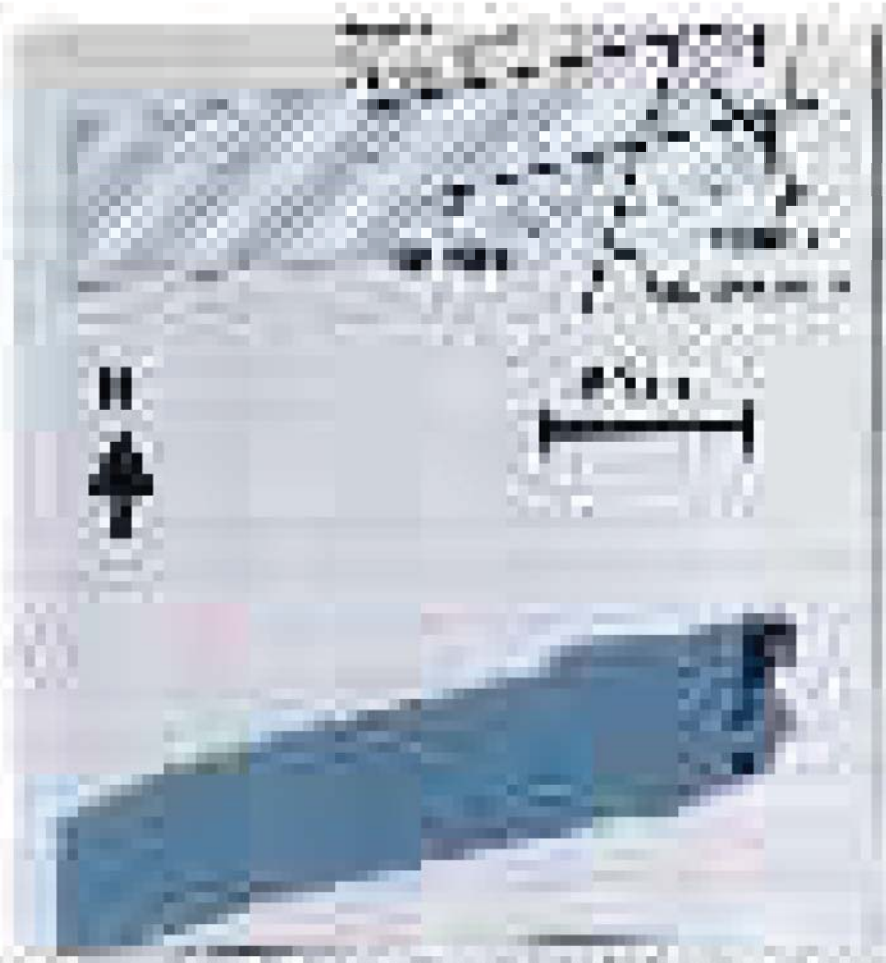
persistence and usually do not contain any secondary minerals. Some of the Group IV fractures contain a whitish gouge similar to that of the Group III fractures. This leads to the interpretation that these joints were sheared as a result of mining activity at a later stage.

Group V: This group lies at roughly 130° to the strike of the face at a steep angle of dip. These joints interconnect with Group VI fractures to form distinctive hackly hangingwall.

Group VI: This group is relatively uncommon and is generally associated with the more prominent Group III shear zones. Underground they occur as short (often gouge-filled) faults that terminate against Group III and sometimes Group I fractures.

The fracture patterns developed in the pillar were explained in terms of the complex stress history of the stabilising pillar, indicating that none of them are the products of preconditioning alone. Since 17-24W stabilising pillar was mined only with preconditioning, a comparison of characters and abundances of the fracture groups identified, with and without preconditioning, was not possible.

Although the evidence from the Blyvooruitzicht Gold Mine site was less direct there were strong indications of re-activation of pre-existing fracture surfaces in the preconditioned area. This was most noticeable in the Group III fractures, with evidence of both horizontal and lateral movement at a later stage. In other words, the reactivation of Group III shears through induced stress redistribution by mining activity with preconditioning was evident. Formation of Group IV and Group VI faults were associated with this shear movement and the stress release immediately ahead of the face by preconditioning. Certain Group IV and VI fractures within the shear zones of Group III changed their character from fine joints into millimetre thick bands of crushed quartzite gouge, indicating that further movement had occurred along the fracture plane. There was strong evidence to suggest that the direction of propagation of seismic events directly after the preconditioning blasts was in the same orientation as that of the Group III fractures (Figure 4.2.15). This further indicated that the mechanism of stress redistribution was by re-activation of existing fractures.



velocity (Maxwell and Young, 1995). According to Maxwell and Young, zones of concentrated seismic activity have been found to be associated with zones of anomalously high velocity, while low-velocity zones tend to be aseismic.

A seismic tomography experiment was performed at experimentation site (17/24W stability pillar) at Blyvooruitzicht Gold Mine to characterise the site in terms of a controlled-source seismic velocity image. The velocity survey was repeated after a preconditioning blast in panel 1 in an attempt to assess the associated effects on the stress state of the pillar.

The footwall and hangingwall drives to the north and south of the pillar were used for the survey. A series of 30 moderately downward-dipping 3 m long boreholes spaced at between 2-3 m were drilled into the south sidewall of the footwall drive. Hydrophone sensors were placed in each of these water-filled holes. Similarly, a series of 35 upward-dipping boreholes was drilled into the north sidewall of the hangingwall drive. During the surveys, individual explosions (generated by single cartridge of Tovex emulsion explosive) were detonated in each of these holes in turn. The blasts were recorded on a seismometer monitoring the hydrophone sensors and the exact detonation time for each blast was measured at the source. The acquisition geometry resulted in dense ray coverage of the survey area (Cameiro, 1995).

Some 1070 P-wave travel-times to each hydrophone were computed by visually picking the arrival-times (Maxwell and Young, 1995). Good signal-to-noise ratios and clear onsets were evident in the waveforms obtained from each sensor and the travel-times were accurately measured to within two samples on average (Maxwell and Young, 1995). Similar quality data were acquired from an accelerometer sensor mounted directly on the tunnel wall surface. This showed that the fracturing around the tunnel extended beyond the ends of the hydrophone holes, so that similar signal attenuation was experienced at both sensor positions.

Using the surveyed locations of the blast and sensor boreholes, the apparent velocities for the rockmass were computed on the assumption of straight ray paths between source and receiver through the pillar (Maxwell and Young, 1995).

Significant velocity variations were detected in the pillar, with velocities of between 4.96 and 6.00 km/s being measured, the average value being 5.67 km/s (standard deviation 0.16 km/s). Figure 4.2.16 shows the variation in velocity from east to west, measured directly across the pillar between common source and receiver holes. A low-velocity zone in the east, corresponding to the open stope, is evident in the figure; ahead of the face, there is a region of increased velocity, corresponding to the expected high-stress anomaly in the pillar. Beyond this, there is a region of lower velocity, followed by a second region of moderately high velocity.

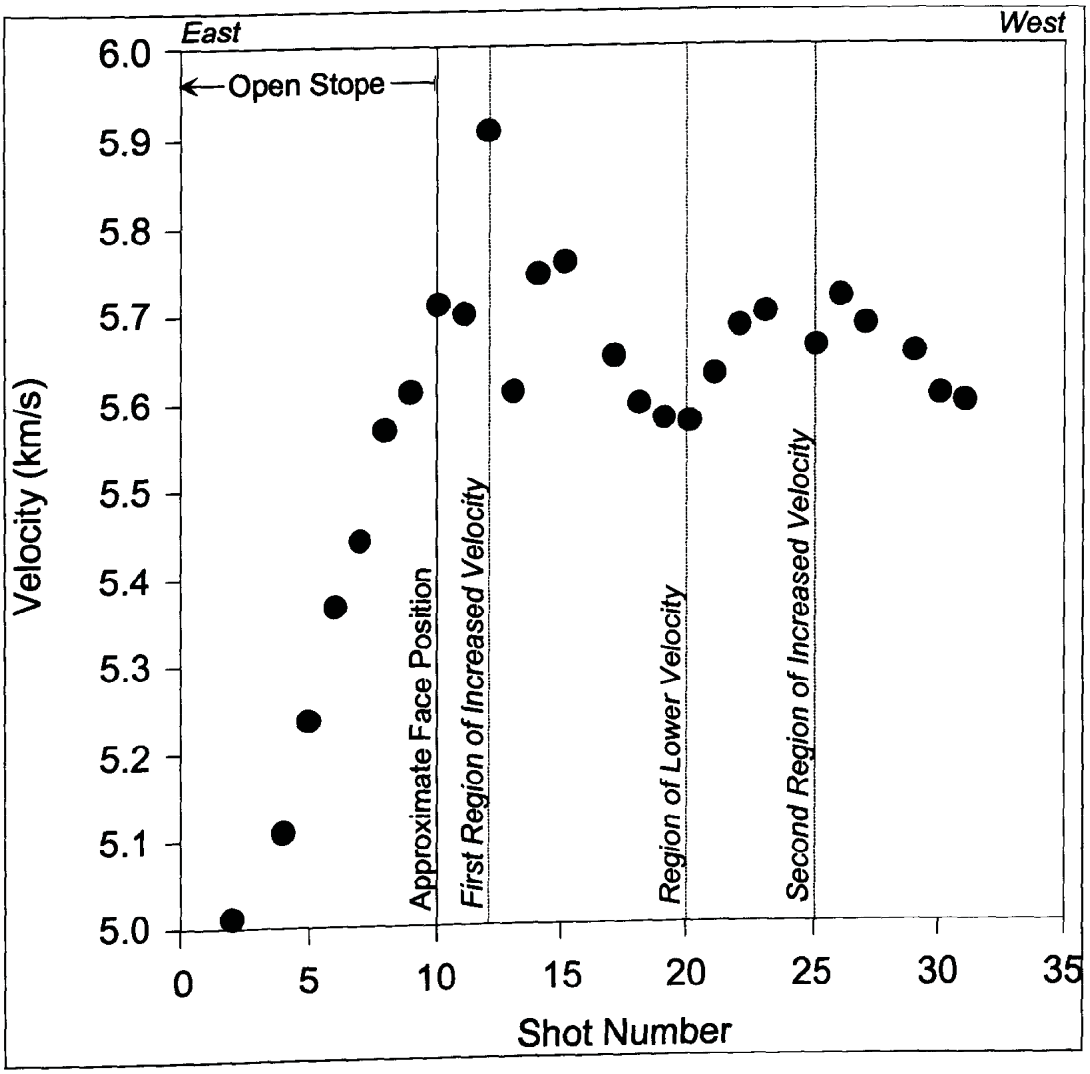


Figure 4.2.16 Plot of the straight ray apparent velocity measured between common shot and receiver hole numbers, showing the velocity variation from east to west (after Maxwell and Young, 1995)

A pervasive apparent-velocity anisotropy (i.e. the apparent velocity has different values in different directions through the rockmass) of some 7.5 per cent was found consistently throughout the data set (Maxwell and Young, *1995*). The *fast* direction was parallel to strike, while the apparent velocity was slower in the dip direction. The anisotropy was most likely produced by the strongly developed alignment of fracturing which was observed parallel to the top and bottom edges of the pillar. A correction was applied to the data to minimise the influence of the anisotropy on the inversion to the velocity image.

A velocity image with a 5-by-10 metre resolution (Figure 4.2.17) was produced by inverting the travel-times. The tunnels used for acquisition are indicated, as is the outline of the unmined pillar. The locations of seismic events recorded during the period of the survey are shown by the small dots. The circled letters are at regions of interest. The maximum estimated stochastic errors were 0.1 km/s and these were reduced to 0.06 km/s in the relatively well-resolved central portion of the image (Maxwell and Young, 1995). The image shows low velocities in and around the open stope ('A' in Figure 4.2.17), where the ray paths either propagated through the (closed) excavation or were diffracted around the stope face. According to Maxwell and Young (1995), the low-velocity anomaly was smeared to the footwall and hangingwall drives due to the limited ray path coverage in the corners of the image.

A high-velocity region extends from north to south across the pillar ahead of the stope face in the image ('B' in Figure 4.2.17). This increased velocity can be attributed to the expected stress increase ahead of the advancing face. The mining-induced seismicity recorded by the monitoring PSS during the period of the surveys tended to concentrate in this high-velocity region, as can be seen in Figure 4.2.17. The highest velocities were found in the southern portion of this region, ahead of the face between panel 2 and the advance heading (stub). This was an area of the pillar that was believed to be ineffectively preconditioned because of the geometries of the panel 2 and the stub preconditioning holes, as *well as the influence* of the stemming at the collars of the holes. It was the site of a large (M=2.3) damaging seismic event in April 1994, after the stub was preconditioned out of sequence before the preconditioning of panel 2. This

appeared to add to the stress concentrated in the area and trigger the failure of the instability.

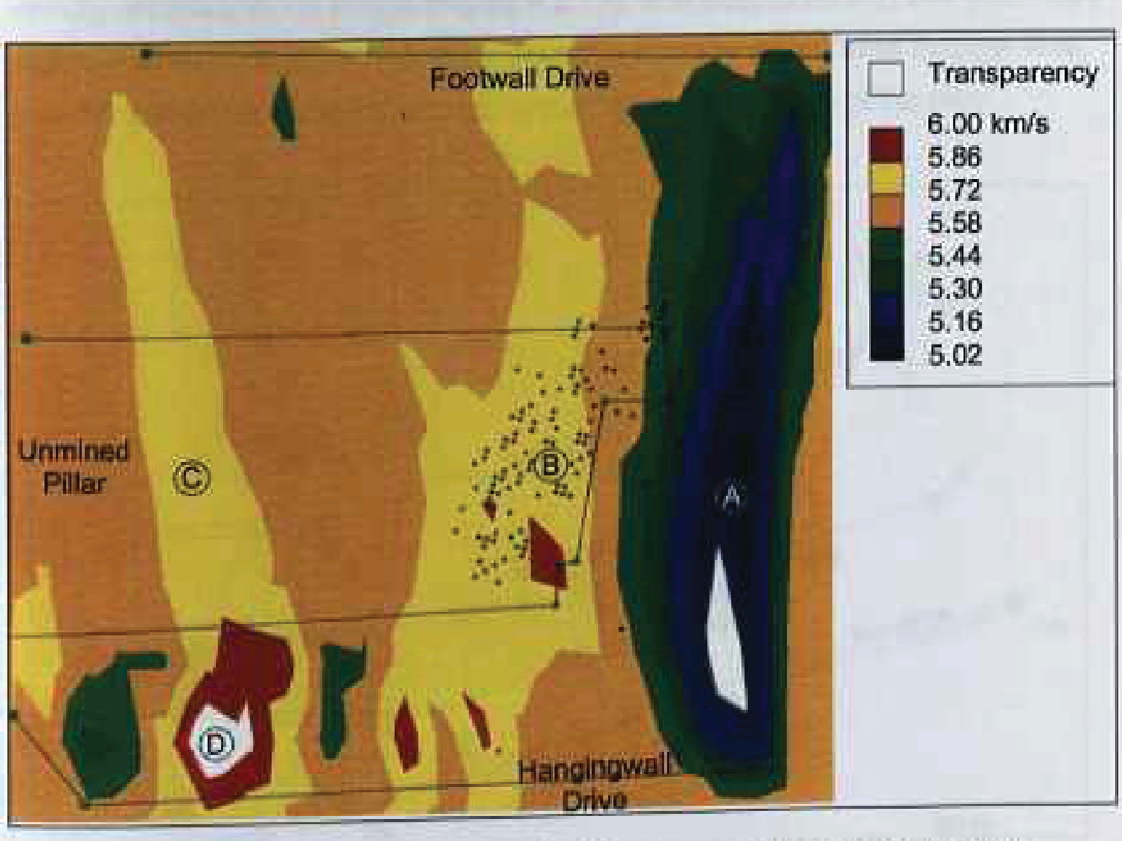


Figure 4.2.17 Straight ray velocity image produced from the seismic tomography survey (after Maxwell and Young, 1995)

Within the pillar, the image shows a second moderately high velocity anomaly, roughly 50 metres ahead of the stope face ('C' in Figure 4.2.17), which appears to correspond to a secondary stress anomaly. Both of the high-velocity regions extend from the footwall drive to the hangingwall drive in the image: according to Maxwell and Young (1995), ray path smearing was to be expected in the north-south direction from the acquisition geometry. A secondary cluster of seismic activity was observed within the core of the pillar. Figure 4.2.18 shows the locations of the larger (M>1.0) seismic events, which were recorded by the PSS prior to this seismic tomography experiment. Figure 4.2.18 shows the locations in plan, while Figure 4.2.19 shows a time section in which the locations of the events through time are projected onto the line *A–B* in Figure 4.2.18. As can be seen in Figure 4.2.18, most of the events were located in the pillar ahead of and relatively close to the advancing stope faces, while the three events highlighted

by stars in the figure were located between 50 and 100 metres ahead of the faces. This observation tended to confirm the presence of the secondary high-velocity anomaly in the image (Figure 4.2.17), and suggested that this secondary region of stress concentration was advancing with the stope faces through time, possibly indicating a degree of progressive failure of the core of the pillar.

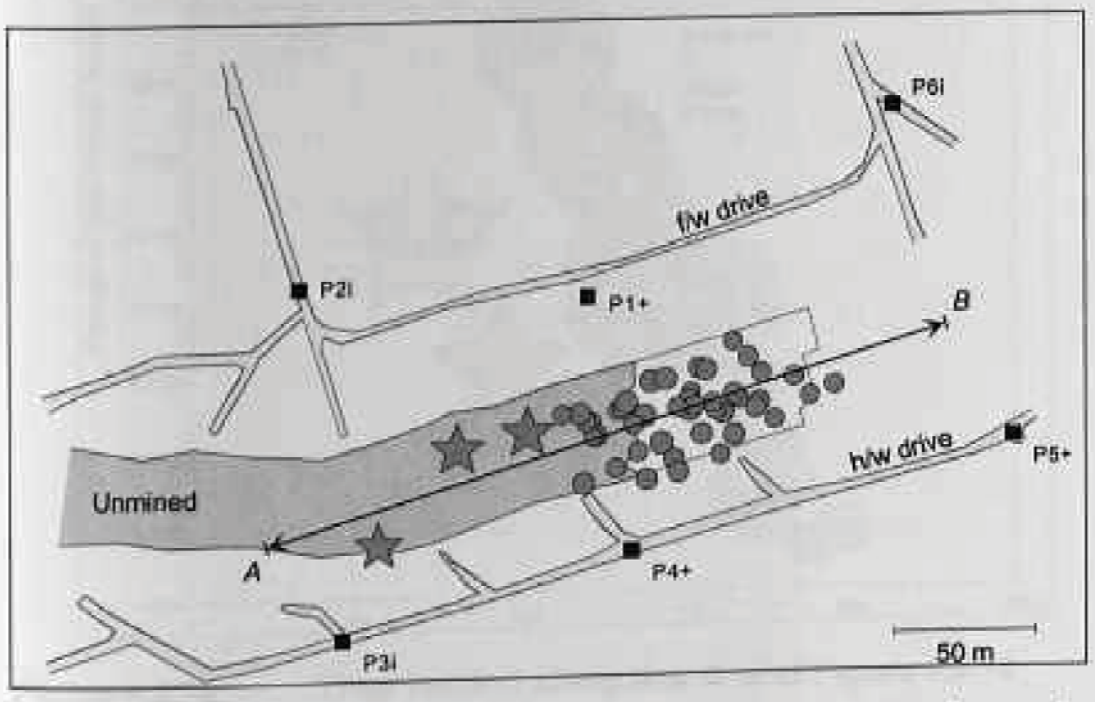


Figure 4.2.18 Plan of the locations of the larger seismic events recorded prior to seismic tomography experiment

The series of alternating high- and low-velocity regions along the southern boundary of the image ('D' in Figure 4.2.17) appeared to be localised, near-shot velocity variations; the average velocities showed a similar, consistent trend over a number of shot holes (Maxwell and Young, 1995). The velocity anomalies were thought to coincide with regions of relatively more and less fractured rock between the hangingwall drive and the pillar.

Carneiro (1995) reprocessed the travel-time data, using a curved ray tracing algorithm, which caters for the effects of refraction of the seismic waves as they pass through the rockmass between source and receiver. The 5-by-10 metre pixels used by Maxwell and Young (1995) were thought to introduce interpolation-related numerical artifacts into the resulting image. The resolution of the image was improved by subdividing the surveyed area into 1-by-1 metre

pixels, ensuring that almost every pixel was crossed by at least one ray path. The resultant image (Figure 4.2.20) was similar to that produced by Maxwell and Young, but without the interpolation artifacts and with a clearer definition of the high-velocity regions.

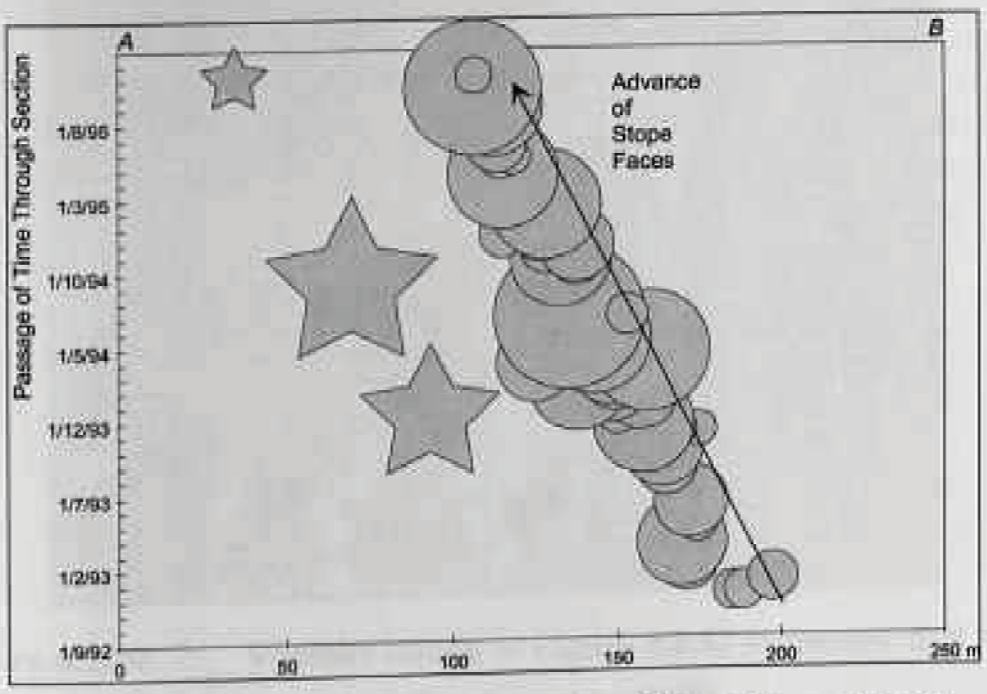


Figure 4.2.19 Time section along line *A–B* of Figure 4.2.18

The velocity survey was repeated after a preconditioning blast in panel 1. According to Maxwell and Young (1995), the preferred method for computing velocity changes between consecutive surveys was to invert the travel-time changes measured by cross-correlating common ray paths (i.e. comparing the waveforms on a mathematical basis). This was thought to be more accurate and precise than simply subtracting the two velocity images, each of which had its own relatively high errors.

Unfortunately, the source explosions for the tomography did not generate signals with the desired degree of repeatability. Probably, the local fracturing produced in the boreholes by the repeated blasts resulted in variations in the energy transfer from the explosive to the rock. The estimated data uncertainty was thus of the same order as the observed variability in the measurements, so that there was considerable uncertainty as to whether any significant velocity changes would be detectable with such imprecise measurements (Maxwell and Young, 1995).

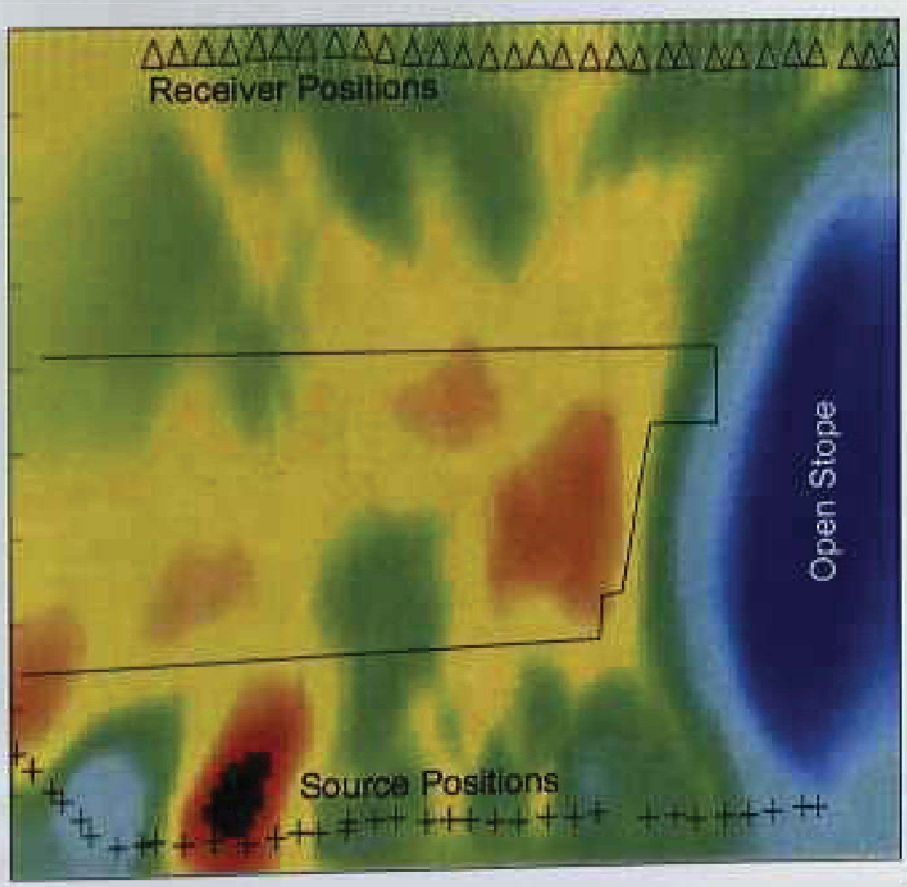


Figure 4.2.20 Velocity image of Figure 4.2.17 reconstructed through curved ray tracing (after Carneiro, 1995)

The imaged velocity-changes (Figure 4.2.21) show velocity variations from -0.22 km/s to +0.20 km/s (measured with respect to a datum of 5.65 km/s), with an estimated maximum error of 0.16 km/s (0.08 km/s in the centre of the image). The alternating high- and low-velocity regions at the northern boundary of the image ('A' in Figure 4.2.21) were thought to be noise-related, as the anomalies were smaller than the error in this portion of the image and were thus not significant. However, the velocity increase of 0.12 km/s near the top of the pillar ('B' in Figure 4.2.21) was probably significant (being larger than the error in that portion of the image), and indicated an increase in stress ahead of panel 1 and into panel 2 as a result of the transfer of stress away from the vicinity of the preconditioning blast. The seismicity recorded by the PSS after the preconditioning blast migrated away from the blast location in panel 1, as shown in Figure 4.2.22, confirming the interpretation of stress transfer by preconditioning.